IB 2020-26

Re-visiting the theoretical investigation of the near wake for turbulent wake flows at zero-pressure gradient

Tobias Knopp, Christopher G. F. Scholl

DLR Deutsches Zentrum für Luft- und Raumfahrt

Berichts.-Nr.: **DLR-IB-AS-GO-2020-26**

Verfasser: Tobias Knopp, Christopher G. F. Scholl

Titel: Re-visiting the theoretical investigation of the near wake for turbulent wake flows at zero-pressure gradient

Datum:

Auftraggeber:

Auftrags-Nr.:

Vorgesehen für:

Der Bericht umfaßt:

32 Seiten einschl.
1 Tabellen
11 Bilder
18 Literaturstellen

D L R

Institut für Aerodynamik und Strömungstechnik
Bunsenstraße 10
37073 Göttingen
Deutschland

Abteilung AS-CAS

DLR

Titel: Re-visiting the theoretical investigation of the near wake for turbulent wake flows at zero-pressure gradient

Übersicht/Abstract: This report re-visits a theoretical investigation for the symmetric wake of a flat plate turbulent boundary layer at zero pressure gradient. The focus is on the near wake, which is the region, where the remnant of the universal mean velocity profile of the inner 15% of the boundary layer still can be observed. The remnant of the universal wall-law, i.e., the universal log-law, is eaten up starting from the centerline, as the flow evolves downstream. The streamwise extent of this region is around 7 to 10 boundary layer thicknesses. Alber (1980) gives an analytical formula for the streamwise development of the centerline velocity and an analytical description of the mean velocity profiles. He derives a similarity solution for the mean velocity profile for the inner 15% of the wake, the region typically occupied by the log-law of the flat plate, in the form of an asymptotic expansion. The similarity transformation involves an inner-layer length scale g, which is the perturbation parameter of the asymptotic expansion. The theory by Alber (1980) has several crucial points, which require special care from a mathematical of point. One of the crucial elements is the order of magnitude analysis based on the inner wake characteristic length scale g. This is studied in more depth in this work. Moreover, the experimental data by Ramaprian & Patel (1982) are re-visited to compare with the theoretical results.
The motivation for this study is to validate and to improve turbulence models based on the RANS approach for the flow phenomenon of wake flow at adverse pressure gradient. Modern transport aircraft employ high-lift systems to provide the necessary lift for low-speed operations during take-off and landing. One critical flow feature of high-lift configurations are confluent flows of the wake of an upstream located element and the boundary layer on downstream located elements, subjected to a strong adverse pressure gradient. For some settings of the flap, the lift stall at high incidence angles can be caused by flow reversal of the wake of the main element above the flap. This is called off-surface flow reversal. The work presented in this report is part of the joint project "Turbulent Wake Flow at Adverse Pressure Gradient" between the Center for Computer Applications in AeroSpace Science and Engineering ($C^2A^2S^2E$) at the DLR Institute of Aerodynamics and Flow Technology (DLR AS), the Institute of Fluid Mechanics (ISM) at Technische Universität Braunschweig, and Peter the Great St. Petersburg Polytechnic University (SPbPTU). This project of the author together with Prof. R. Radespiel and Dr. P. Scholz from ISM and with Prof. M. Strelets from SPbPTU was funded by DFG and the Russian Foundation for Basic Research (RFBR) under Grant No. RA 595/26-1, KN 888/3-1 and No. 17-58-12002.

DEUTSCHES ZENTRUM FÜR LUFT- UND RAUMFAHRT E.V.

Institut für Aerodynamik und Strömungstechnik

Institutsleiter::

(Prof. Dr. Andreas Dillmann)

Verfasser:

Tobias Knopp

(Dr. Tobias Knopp)

Abteilungsleiterin:

Cornelia Grabe

(Dr. Cornelia Grabe)

Datum: 18.02.20 Bearbeitet:	Abteilung: AS-CAS	Bericht: IB-AS-GO-2020-26

Contents

Chapter 1

Introduction

The work presented in this report is part of a joint project "Turbulent Wake Flow at Adverse Pressure Gradient" between the Center for Computer Applications in AeroSpace Science and Engineering at the DLR Institute of Aerodynamics and Flow Technology, the Institute of Fluid Mechanics (ISM) at Technische Universität Braunschweig, and Peter the Great St. Petersburg Polytechnic University (SPbPTU). This project of the author together with Prof. R. Radespiel and Dr. P. Scholz from ISM and with Prof. M. Strelets from SPbPTU is funded by DFG and the Russian Foundation for Basic Research (RFBR) under Grant No. RA 595/26-1, KN 888/3-1 and No. 17-58-12002.

Modern transport aircraft employ high-lift systems to provide the necessary lift for low-speed operations during take-off and landing. Transport aircrafts use a combination of a leading edge slat and a trailing edge single slotted Fowler flap as the state-of-the-art system. The CFD-based design process of high-lift systems is still very challenging. While RANS based computational flow simulation is an integrated part of wing design for cruise flight, reliability and maturity for high-lift at low-speed has not yet been achieved. One major reason for this is the lack of predictive accuracy of current RANS turbulence models near maximum lift. Critical flow features are turbulent boundary layer flows, wake flows of elements located upstream, and the confluent flow of upstream element wakes and boundary layers on downstream elements, all subjected to a strong adverse pressure gradient (APG), cf. Ying et al. [1996], C. L. Rumsey [2002]. The lift stall at high incidence angles can also be caused by flow reversal of the wake of the main element due to the adverse pressure gradient caused by the flap, see Rumsey and Gatski [1999]. This is also called off-surface separation or off-surface flow reversal.

The flow phenomenon of a wake subjected to an adverse pressure gradient was studied in isolation e.g. by Driver and Mateer [2002]. They performed a new wind tunnel experiment and compared the measurements with RANS simulations. They report that present eddy-viscosity based standard RANS models (Spalart-Allmaras and Menter SST k-ω) significantly under-predict the tendency for flow reversal due to APG observed in the experiments. However, there are some open questions about this experiment. Therefore within this joint project, SPbPTU performed a numerical experiment using large-eddy simulations of the test-case by Driver and Mateer. The aim was to assess the role of details of the wind-tunnel experiment on the appearance of flow rever-

sal, e.g., role of the jet-actuation at the wind-tunnel walls which generates the APG, shear layer instability in the far wake, three-dimensional side wall effects. These results are published in Guseva et al. [2019] and Guseva et al. [2018]. The numerical experiment was then used as a test-case for RANS simulations. The RANS results by Burnazzi et al. [2018] confirmed the findings by Driver and Mateer [2002]. This reveals that RANS turbulence models need to be modified for more accurate prediction of the flow phenomenon of wake flow at APG.

The theoretical investigation for the symmetric wake of a flat plate turbulent boundary layer at zero pressure gradient was presented by Alber [1980]. His focus on the near wake, which is the region, where remnants of the universal velocity profile of the inner 15% of the boundary layer still can be observed. The remnants are eaten up, as the flow evolves downstream. Alber distinguishes between the near wake region I, where the remnants of the viscous sublayer are eroded, and the near wake region II, where the remnants of the log-law are eroded. Following Alber, the streamwise extent of region I is around 10 viscous sublayer thicknesses, and the extent of region II is around 7 to 10 boundary layer thicknesses. Alber gives an analytical formula for the streamwise development of the centerline velocity and analytical description of the mean velocity profiles. Alber [1980] gives a similarity solution for the mean velocity profile for the inner 15% of the wake, the region typically occupied by the log-law of the splitter plate, in the form of an asymptotic expansion. The similarity transformation involves an inner-layer length scale g, which is the perturbation parameter of the asymptotic expansion. Note that in the prior work by Alber [1980] and Ramaprian et al. [1982] only the first order approximations are shown for the validation of the theory by experimental data. In this work, also the second order approximation is computed and plotted.

The theory by Alber [1980] has several crucial points, which require special care from a mathematical of point. One of the crucial elements is the order of magnitude analysis based on the inner wake characteristic length scale g. This is studied in more depth in this work. We could show that the assumption made implicitly by Alber [1980] for simplification is satisfied for high Re flows with $Re_x > 10^7$. Moreover, Albers theory gives a theoretical relation for the centerline velocity in the form. In this work, the experimental data are revisited.

Experimental studies of the wake of a thin flat plate and its boundary layer were performed by Chevray and Kovasznay [1969]. These are the data used by Alber for the validation of his theory. Thereafter the experiments by Ramaprian et al. [1982] were made.

Regarding further theoretical studies and refinement of the work by Alber [1980], we mention the work by Bogucz and Walker [1988]. An earlier work was given by Robinson [1967]. He proposed a similarity solution in a turbulent mixing layer and in a turbulent wake developing from an initial turbulent boundary layer.

The motivation for this review of the theoretical work by Alber is to gain insight and to develop ideas for a modification of RANS turbulence models for the near-wake at APG. This was accompanied by the design of a new test-case of a wake at adverse pressure gradient and the setup of a database by a joint investigation of a wind-tunnel experiment, see Breitenstein et al. [2019] and a numerical experiment, see Guseva et al. [2019].

This approach will take the following steps:

(i) Extension of the work for ZPG to APG by assuming that the log-law for ZPG needs to be replaced by a square-root law found for turbulent boundary layers at adverse pressure gradient, see Knopp et al. [2017].

(ii) Investigation and validation of the modelling assumptions of step (i) using new data by Breitenstein et al. [2019] and Guseva et al. [2019]

(iii) Develop a turbulence model correction term, most likely for the length scale equation, which is the ω-equation for the SSG/LRR-ω model. This approach to develop a correction term based on inverse modelling for a simplified boundary layer problem, which only accounts for the most relevant terms of the ω-equation, has been demonstrated for turbulent boundary layers at APG in Knopp [2016] and Knopp et al. [2018].

(iv) Validation of the modified RANS model using the experimental and numerical data by Breitenstein et al. [2019] and Guseva et al. [2019].

The present work showed that the mathematical complexity of the ZPG case is already quite challenging. An in-depth understanding of the ZPG case turned out to be important for the extension to APG. Albeit first attempts on this have been made, this is still subject to future research.

Table 1.1: Nomenclature used in this work

B	log-law intercept, [-]
c_f	skin friction coefficient, [-]
C_L	lift-force coefficient, [-]
c_p	pressure coefficient, [-]
P	mean pressure, [kg/(ms^2)]
U	wall parallel mean velocity, [m/s]
u^+	mean velocity in viscous units using u_τ and ν, [-]
$u^+_{\log}$	logarithmic law (log-law) for u^+, [-]
u^+_{sqrt}	square-root law (sqrt-law) for u^+, [-]
u_τ	friction velocity, [m/s]
$\overline{u'v'}$	correlation of wall parallel velocity fluctuation u' and wall normal fluctuation v', [m^2/s^2]
V	wall normal mean velocity, [m/s]
Re_c	Reynolds number based on the chord c, [-]
Re_θ	Reynolds number based on the momentum thickness, [-]
Re_τ	Reynolds number based on the friction velocity u_τ, [-]
x	wall tangential coordinate in a wall-fitted coordinate system, [m]
y	wall normal coordinate in a wall-fitted coordinate system, [m]
Greek	
α	incidence angle, [°]
δ_{99}	boundary layer thickness, [m]
Δp_x^+	pressure gradient parameter, [-]
κ	log-law slope for zero-pressure gradient turbulent boundary layer flows, [-]
ν	kinematic viscosity, [m^2/s]
ν_t	turbulent viscosity [m^2/s]
μ	dynamic viscosity [kg/(ms)]
ρ	density, [kg/m^3]
θ	displacement thickness, [m]
τ_w	wall shear stress, [N/m^2]
Subscripts	
log	logarithmic layer
sqrt	square-root layer
apg	adverse pressure gradient
Superscripts	
+	quantity scaled in viscous units using u_τ and ν
Abbreviations	
APG	adverse pressure gradient
RANS	Reynolds averaged Navier-Stokes
T.E.	Trailing edge (of the splitter plate)

Chapter 2

Turbulent logarithmic near wake

2.1 Nomenclature compared to work by Alber

Alber [1980] uses the notation that dimensional mean-flow quantities are denoted by small letters with a superscript $*$. Mean-flow quantities are made non-dimensional using the friction velocity and the kinematic viscosity and are denoted by small letters but without the superscript $+$. In this work we use the convenient notation using the superscript $+$ to denote inner viscous scaling.

2.2 Boundary layer approximation for the near wake

We focus on the so-called region II of the near wake, as denoted in the work by Alber [1980]. It is the region where remnats of the log-law region of the upstream boundary layer still can be observed. The remnants of the log-law are eaten up, as the flow evolves downstream.
In his work, Alber [1980] uses the following boundary layer equations, which he uses in the non-dimensional form scaled to plus-units

$$\frac{\partial u^+}{\partial x^+} + \frac{\partial v^+}{\partial y^+} = 0 \tag{2.1}$$

$$u^+ \frac{\partial u^+}{\partial x^+} + v^+ \frac{\partial u^+}{\partial y^+} = \frac{\partial}{\partial y^+}\left[\nu_t^+ \frac{\partial u^+}{\partial y^+}\right] \tag{2.2}$$

However, note that Alber [1980] does not use the superscript $+$ in his work. Therein the following assumptions are used: (i) the streamwise pressure gradient is assumed to be negligible small, i.e. $\mathrm{d}p/\mathrm{d}x = 0$; (ii) the turbulent diffusion of momentum is much larger than the laminar mixing; (iii) the Boussinesq assumption is used to model the turbulent shear stress.

Equation (2.2) corresponds to equation (32) in Alber [1980]. Note that in this work we include the superscript $+$ indicating plus units. The inner viscous plus-scaling uses the friction velocity at the trailing edge (T.E.) of the upstream

turbulent boundary layer. Alber [1980] uses the following form for turbulent viscosity hypothesis

$$\nu_t^+ = \kappa y^+ \tag{2.3}$$

Alber [1980] seeks a solution of the momentum equation and the continuity equation which is valid for large x such that, for a fixed value of x,

$$\lim_{y^+\to\infty} u^+ = \frac{1}{\kappa}\log(y^+) + B \tag{2.4}$$

2.3 Similarity solution for the near wake

2.3.1 Ansatz for a similarity solution

Alber [1980] proposes to seek a similarity solution of the form

$$u^+(x^+, y^+) = S(x^+) + \frac{1}{\kappa}F'(\eta), \qquad \eta = \frac{y^+}{g(x^+)} \tag{2.5}$$

Therein the velocity contribution S is closely related to the centerline velocity scaled in plus units. The velocity contribution F' is also scaled in plus units. The function g is a non-dimensional length scale suitable for the inner region of the near wake region II and needs to be specified. Primes denote differentiation w.r.t. η or x^+.

2.3.2 Similarity equation for the mean velocity

Using the chain rule for differentiation, the derivative $\partial u^+/\partial x^+$ is given by

$$\frac{\partial u^+}{\partial x^+} = S' + \frac{1}{\kappa}F''(-)\frac{y^+}{g^2}g' = S' - \frac{1}{\kappa}F''\eta\frac{g'}{g} \tag{2.6}$$

and that $\partial u^+/\partial y^+$ is given by

$$\frac{\partial u^+}{\partial y^+} = \frac{1}{\kappa}F''\frac{1}{g} \tag{2.7}$$

Then Alber [1980] uses the continuity equation to determine v^+. We writes $y^+ = y^+(\eta) = g(x^+)\eta$ and obtains

$$\begin{aligned} v^+ = -\int_0^{y^+}\frac{\partial u^+}{\partial x^+}\mathrm{d}y^+ &= -S'y^+ + \frac{1}{\kappa}\int_0^{y^+} F''\eta\frac{g'}{g}\mathrm{d}y^+ \\ &= -S'g\eta + \frac{1}{\kappa}\int_0^{y^+(\eta)} F''\eta\frac{g'}{g}\mathrm{d}y^+ \\ &= -S'g\eta + \frac{1}{\kappa}\int_0^{\eta} F''\eta\,\frac{g'}{g}g\mathrm{d}\eta \\ &= -S'g\eta + \frac{1}{\kappa}g'\int_0^{\eta} F''\eta\mathrm{d}\eta \end{aligned} \tag{2.8}$$

Moreover we use integration by parts $\int f'h = -\int fh' + [fh]$ with $f' = F''$, $f = F'$, $h = \eta$ and $h' = 1$ to obtain

$$\int_0^\eta (F''\eta)\,\mathrm{d}\eta = -\int_0^\eta F'\mathrm{d}\eta + [F'\eta]_0^\eta = F'\eta - F \tag{2.9}$$

This gives us finally

$$v^+ = -S'\eta g + \frac{1}{\kappa}g'\left(\eta F' - F\right) \tag{2.10}$$

which is equation (35) in the work by Alber [1980].

Substitution of (2.10) into the momentum equation (2.2) gives

$$u^+\frac{\partial u^+}{\partial x^+} + v^+\frac{\partial u^+}{\partial y^+} = \frac{\partial}{\partial y^+}\left[\nu_t^+\frac{\partial u^+}{\partial y^+}\right] \tag{2.11}$$

This can be written as

$$\begin{aligned}&\left(S + \frac{1}{\kappa}F'\right)\left(S' - \frac{1}{\kappa}F''\eta\frac{g'}{g}\right)\\ &+\left(-S'\eta g + \frac{1}{\kappa}g'\left(\eta F' - F\right)\right)\left(\frac{1}{\kappa}F''\frac{1}{g}\right) = \frac{\partial}{\partial y}\left(\kappa y\frac{1}{\kappa}F''\frac{1}{g}\right)\end{aligned}$$

This can be rearranged as

$$\begin{aligned}&SS' + \frac{1}{\kappa}F'S' - \frac{1}{\kappa}SF''\eta\frac{g'}{g} - \frac{1}{\kappa}F'\frac{1}{\kappa}F''\eta\frac{g'}{g}\\ &\quad -S'\eta g\frac{1}{\kappa}F''\frac{1}{g} + \frac{1}{\kappa}g'\left(\eta F' - F\right)\frac{1}{\kappa}F''\frac{1}{g} = F''\frac{1}{g} + F'''\frac{y^+}{g^2}\end{aligned}$$

leading to

$$\begin{aligned}gSS' + \frac{g}{\kappa}F'S' - \frac{g'}{\kappa}S\eta F'' - \frac{1}{\kappa^2}g'\eta F'F'' - \frac{g}{\kappa}S'\eta F''\\ + \frac{1}{\kappa^2}g'\left(\eta F' - F\right)F'' = F'' + \eta F'''\end{aligned} \tag{2.12}$$

which can be rearranged as

$$\begin{aligned}[\eta F'']' + \frac{g'}{\kappa}S[\eta F''] - gSS' = &\frac{g}{\kappa}S'\left[F' - \eta F''\right] - \frac{1}{\kappa^2}g'\eta F'F''\\ &+ \frac{1}{\kappa^2}g'\left(\eta F' - F\right)F''.\end{aligned}$$

After reduction of the terms on the right hand side we obtain the following equation for which a similarity solution is sought

$$[\eta F'']' + \frac{g'}{\kappa}S[\eta F''] - gSS' = \frac{g}{\kappa}S'\left[F' - \eta F''\right] - \frac{1}{\kappa^2}g'FF'' \tag{2.13}$$

According to Alber [1980], the dominant terms are on the left-hand side of equation (2.13). This claim will be shown below. The requirement for the existence of a similarity solution for F is that the functions appearing as the coefficients of the terms on the left-hand side of equation (2.13) need be equal to constant values. The condition can be relaxed to require that the coefficients become constants for large values of x^+ or g.

2.4 Solution for the inner length scale g

The condition for a similarity solution gives a set of two coupled equations for the inner length scale g and the contribution to the centerline velocity S. Following Alber [1980] the following quantities need to be constant, e.g., independent of x^+:

$$\text{(i)} \quad g'S/\kappa = c_1 \tag{2.14}$$

$$\text{(ii)} \quad g\,S\,S' = c_2 \tag{2.15}$$

which corresponds to equation (37) in the work by Alber [1980]. This is a set of two coupled first order ordinary differential equations for g and S which are functions of x^+. By using (ii) to express $S = c_2/(gS')$ and substitution of S into (i) we obtain

$$\frac{g'\,S}{\kappa} = \frac{c_2 g'}{\kappa g S'} = c_1 \quad \Leftrightarrow \quad \frac{c_2}{\kappa}\frac{g'}{g} = c_1 S' \quad \Leftrightarrow \quad \frac{c_2}{\kappa}\log(g(x^+)) = c_1 S(x^+) \tag{2.16}$$

or rearranged

$$\frac{c_2}{c_1}\frac{1}{\kappa}\log(g(x^+)) = S(x^+) \tag{2.17}$$

which is equation (38) in Alber [1980]. This relation is then substituted into condition (ii), i.e., into equation (2.15), to obtain

$$\begin{aligned} g\,S\,S' = g\frac{c_2}{c_1}\frac{1}{\kappa}\log(g)\frac{c_2}{c_1}\frac{1}{\kappa}\frac{g'}{g} = c_2 \quad &\Leftrightarrow \quad \frac{c_2}{c_1^2}\frac{1}{\kappa^2}\log(g)g' = 1 \\ &\Leftrightarrow \quad \log(g)g' = \frac{c_1^2}{c_2}\kappa^2 \end{aligned} \tag{2.18}$$

i.e., we obtain the following ordinary differential equation for g (see equation (39) in the work of Alber [1980])

$$\log(g(x^+))g'(x^+) = \frac{c_1^2}{c_2}\kappa^2 \tag{2.19}$$

We then use the following form for the integral of $\log(g)g'$, viz.,

$$\frac{\mathrm{d}}{\mathrm{d}x^+}\left[g\left(\log(g)-1\right)\right] = g'\left(\log(g)-1\right) + g\frac{g'}{g} = g'\log(g) - g' + g' = g'\log(g) \tag{2.20}$$

Therefore the integration of (2.18) leads to

$$g[\log(g)-1] = \frac{c_1^2}{c_2}\kappa^2 x \tag{2.21}$$

where we follow Alber [1980] and use the boundary condition $g(0) = e^1$. From equation (2.19) we see that

$$g(0) = e^1 \quad \Leftrightarrow \quad S(0) = \frac{c_2}{c_1}\frac{1}{\kappa} \tag{2.22}$$

2.4.1 Solution for the inner length scale

By using the tool Wolfram alpha and its routine "solve and equation in terms of x & y for y" for the expression $y(\log(y)-1) == c_1^2/c_2\kappa^2 x$ we obtain for $y \equiv g$

$$g(x^+) = e^{W_0\left(\frac{c_1^2}{c_2}\frac{\kappa^2}{e}x^+\right)+1}, \qquad x > 0 \tag{2.23}$$

where W_0 is the Lambert W-function. W_0 is the inverse function of $f(z) = ze^z$, i.e.,

$$f \circ f^{-1}(z) = \mathrm{Id}(z) \quad , \qquad f(z) = ze^z \quad , \qquad f^{-1} = W_0 \tag{2.24}$$

where $\mathrm{Id}(z) = z$. The problem to determine the solution z of the fix point problem

$$z = W_0(z)e^{W_0(z)} \tag{2.25}$$

can be written as the problem to determine the solution of $\mathcal{F}(z) = 0$ with $\mathcal{F}$ defined by

$$z = W_0(z)e^{W_0(z)} \quad \Leftrightarrow \quad \mathcal{F}(z) = W_0(z)e^{W_0(z)} - z = 0 \tag{2.26}$$

This can be solved iteratively using Newton's method. Starting with an initial guess η_0, determine η_{n+1} given η_n by the relation

$$\eta_{n+1} = \eta_n - \frac{\mathcal{F}(\eta_n)}{\mathcal{F}'(\eta_n)}, \quad \mathcal{F}(\eta) = \eta e^\eta - \eta, \quad \mathcal{F}'(\eta) = (1+\eta)e^\eta \tag{2.27}$$

2.4.2 Discussion of constants

In this section we can set $c_1 = c_2 = 1$ without loss of generality, as claimed by Alber [1980]. First we summarize the solution for S and for S'

$$S(x^+) = \frac{c_2}{c_1}\frac{1}{\kappa}\log(g(x^+)), \qquad S'(x^+) = \frac{c_2}{c_1}\frac{1}{\kappa}\frac{g'(x^+)}{g(x^+)} \tag{2.28}$$

Therein, S is a function of g which is given in terms of the Lambert W-function by (for $x^+ > 0$)

$$g(x^+) = e^{W_0\left(\frac{c_1^2}{c_2}\frac{\kappa^2}{e}x^+\right)+1} \tag{2.29}$$

The derivative g' can be computed using the chain rule for differentiation as follows

$$\begin{aligned} g'(x^+) &= e^{W_0\left(\frac{c_1^2}{c_2}\frac{\kappa^2}{e}x^+\right)+1} W_0'\left(\frac{c_1^2}{c_2}\frac{\kappa^2}{e}x^+\right)\frac{c_1^2}{c_2}\frac{\kappa^2}{e} \\ &= e^1 e^{W_0\left(\frac{c_1^2}{c_2}\frac{\kappa^2}{e}x^+\right)} \frac{W_0\left(\frac{c_1^2}{c_2}\frac{\kappa^2}{e}x^+\right)}{\left(\frac{c_1^2}{c_2}\frac{\kappa^2}{e}x^+\right)\left[W_0\left(\frac{c_1^2}{c_2}\frac{\kappa^2}{e}x^+\right)+1\right]}\frac{c_1^2}{c_2}\frac{\kappa^2}{e} \\ &= \frac{c_1^2}{c_2}\frac{\kappa^2}{\left[W_0\left(\frac{c_1^2}{c_2}\frac{\kappa^2}{e}x^+\right)+1\right]} = \frac{c_1^2}{c_2}\frac{\kappa^2}{\log(g(x^+))} \end{aligned} \tag{2.30}$$

which uses the following relation for the derivative of W_0

$$W_0'(x) = \frac{W(x)}{x\,[W(x)+1]} \tag{2.31}$$

and we use the relation that $e^{W(x)}W(x) = x$. We substitute this solution into the similarity condition (i), see (2.14), and obtain

$$c_1 = \frac{g'\,S}{\kappa} = \frac{1}{\kappa}\frac{c_1^2}{c_2}\frac{\kappa^2}{\log(g(x^+))}\frac{c_2}{c_1}\frac{1}{\kappa}\log(g(x^+)) = c_1 \tag{2.32}$$

and we see that this equation is satisfied for any c_1. Similarly, for condition (ii), see (2.15), we obtain

$$\begin{aligned} c_2 = gSS' &= g(x^+)\frac{c_2}{c_1}\frac{1}{\kappa}\log(g(x^+))\frac{c_2}{c_1}\frac{1}{\kappa}\frac{g'(x^+)}{g(x^+)} = \frac{c_2^2}{c_1^2}\frac{1}{\kappa^2}\log(g(x^+))g'(x^+) \\ &= \frac{c_2^2}{c_1^2}\frac{1}{\kappa^2}\log(g(x^+))\frac{c_1^2}{c_2}\frac{\kappa^2}{\log(g(x^+))} = c_2 \end{aligned} \tag{2.33}$$

which is satisfied for any c_2. From this we see that we can set $c_1 = c_2 = 1$ without loss of generality, as claimed by Alber [1980].

2.4.3 Order of magnitude estimate for the inner length scale g

The inner wake length scale g deserves special attention. The near wake extends up to $x^+ < 10\delta_{99}^+$. Therefore the relevant boundary layer parameter is the friction Reynolds number $Re_\tau = \delta_{99}^+$. Note that we sometimes write $Re_{\tau,\mathrm{T.E.}}$ instead of Re_τ to denote the reference position for taking u_τ, i.e., near the trailing edge (T.E.) of the splitter plate.

For illustration we give the following example

- $Re_{\tau,\mathrm{T.E.}} = 10000$, i.e., $Re_x \approx 12 \times 10^6$ and $Re_\theta \approx 25000$
- Outer edge of log-layer at $y^+ = 1500$
- Streamwise extent of the near wake $x^+ < 10\delta_{99}^+$ where $\delta_{99}^+ = Re_{\tau,\mathrm{T.E.}}$

Then we show g and $\log(g)$ for two cases, (i) for moderate Re and (ii) for high Re. First we study the case at moderate $Re_\tau \approx 1000$ of the boundary layer, see figure 2.1. For $x^+ = 2000 = 2\delta_{99}^+$, g has reached a value of around 100 and $\log(g)$ has reached a value of around 5. Then we study the case at high $Re_\tau \approx 25000$ of the boundary layer, see figure 2.2. Interestingly, for $x^+ = 100000 = 4\delta_{99}^+$, g has reached a value of around 2000. But $\log(g)$ grows much slower and has reached only a value of around 8. From this we see that the case of an asymptotically high Re is reached only slowly. On the positive side, the theory by Alber can already be assessed for moderately high Re flows.

2.5 Order of magnitude discussion for the similarity equation

In the next step Alber [1980] performs an order of magnitude estimate for the different terms of the similarity equation (2.13). For the coefficients on the left

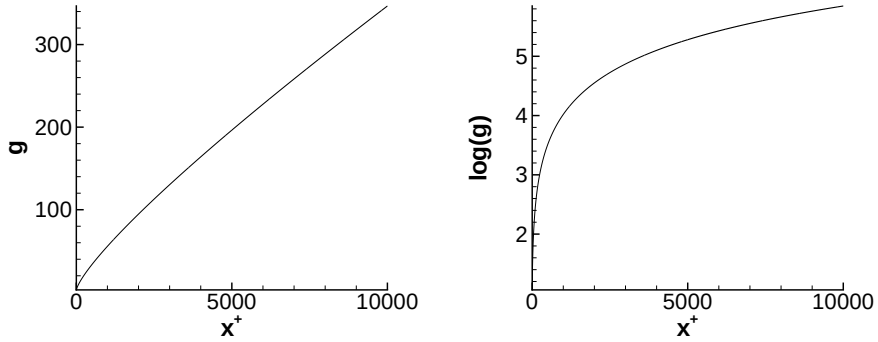

Figure 2.1: Behaviour of g and $\log(g)$ for moderate Re. The near wake extends up to $x^+ < 10\delta_{99}^+$. For this example, let $Re_\tau = 1000$ near the trailing edge. Left: Plot of $g(x^+)$ vs. x^+. Right: Plot of $\log(g(x^+))$ vs. x^+.

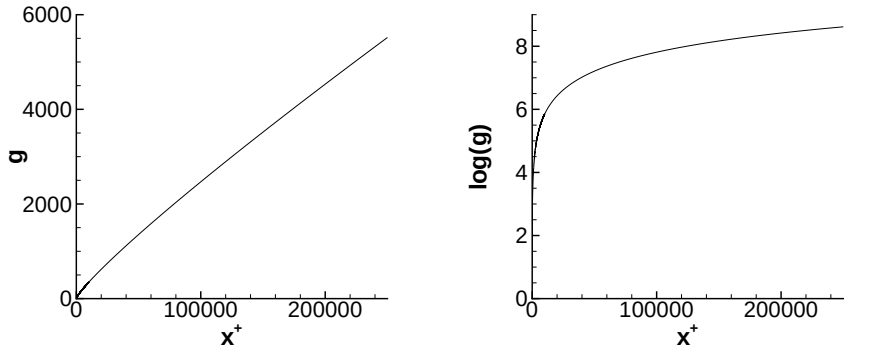

Figure 2.2: Behaviour of g and $\log(g)$ for high Re. The near wake extends up to $x^+ < 10\delta_{99}^+$. For this example, let $Re_\tau = 25000$ near the trailing edge. Left: Plot of $g(x^+)$ vs. x^+. Right: Plot of $\log(g(x^+))$ vs. x^+.

hand side we use (2.14) and (2.15) which gives

$$[\eta F'']' + c_1[\eta F''] - c_2 = \frac{g}{\kappa} S' [F' - \eta F''] - \frac{1}{\kappa^2} g' F F'' \tag{2.34}$$

Regarding the coefficients on the right hand side, the first coefficient can be written as

$$\frac{g}{\kappa} S' = \frac{g}{\kappa} \frac{c_2}{c_1 \kappa} \frac{g'}{g} = \frac{1}{\kappa^2} \frac{c_2}{c_1} g'(x^+) \tag{2.35}$$

Therefore the coefficients of the two terms on the right hand side are the same. Then we use relation (2.18)

$$\log(g)\, g' = \frac{c_1^2}{c_2} \kappa^2 \qquad \Leftrightarrow \qquad \frac{1}{\kappa^2} g' = \frac{c_1^2}{c_2} \frac{1}{\log(g(x^+))} \tag{2.36}$$

and by substitution of this relation into the momentum equation (2.34) we obtain

$$[\eta F'']' + c_1[\eta F''] - c_2 = \frac{c_2}{c_1\kappa^2} g' [F' - \eta F''] - \frac{1}{\kappa^2} g' [FF''] \tag{2.37}$$

Using relation (2.36) this equation can be rearranged as

$$[\eta F'']' + c_1[\eta F''] - c_2 = \frac{c_2}{c_1}\frac{c_1^2}{c_2}\frac{1}{\log(g(x^+))} [F' - \eta F''] - \frac{c_1^2}{c_2}\frac{1}{\log(g(x^+))} [FF''] \tag{2.38}$$

or written in the form of equation (40) in the work of Alber [1980]

$$[\eta F'']' + c_1[\eta F''] - c_2 = c_1\frac{1}{\log(g(x^+))} [F' - \eta F''] - \frac{c_1^2}{c_2}\frac{1}{\log(g(x^+))} [FF''] \tag{2.39}$$

The terms on the right hand side a of order $\mathcal{O}(\log(g(x^+)))$. As described in figure 2.2, $g(x^+)$ is typically of order of magnitude of $\mathcal{O}(10^3)$ or $\mathcal{O}(10^4)$. Therefore $\log(g(x^+))$ is in the range of 5 to 8 for relevant x^+-values, and is (for practical engineering arguments) large compared to 1. Thus the terms on the right hand side are almost one order of magnitude smaller than the terms on the left hand side of (2.39). This leads to the idea of an asymptotic expansion of the solution F'.

2.6 Ansatz of an asymptotic expansion for F'

Alber [1980] proposes the following asymptotic expansion for $F(\eta)$

$$F = F_0(\eta) + \frac{1}{\log(g)} F_1(\eta) + \frac{1}{\log^2(g)} F_2(\eta) + \dots \tag{2.40}$$

Therein Alber makes the assumption of asymptotic expansion that $\log(g) \gg 1$. Recall the result that even for moderate Re (i.e., for example, $Re_\tau = 1000$), $\log(g(x^+)) \approx 5$ for $x^+ = 2\delta_{99}^+$ downstream of the trailing edge of the splitter plate, see figure 2.1. From this we estimate that the contribution of F_1 to F is small compared to the contribution of F_0, but the role of F_1 is not suppressed due to a negligible weight from the expansion parameter. Regarding the contribution of F_2, however, this contribution can be estimated to be small as $\log(g(x^+)) \approx 25$.

Then, from (2.39) it follows that F_0 satisfies the linear equation

$$[\eta F_0'']' + c_1[\eta F_0''] - c_2 = 0 \tag{2.41}$$

and that the equation for F_1 is

$$[\eta F_1'']' + c_1[\eta F_1''] - c_2 = c_1 [F_0' - \eta F_0'' - F_0 F_0''] \tag{2.42}$$

For all other higher order terms F_i ($i \geq 2$), similar equations can be derived. Note that the equations for F_i ($i = 0, 1, \dots$) are all linear.

2.6.1 Boundary conditions

The boundary conditions for F follow from the boundary conditions for u^+ and v^+, where, following Alber [1980],

$$v^+ = 0 \quad \text{for} \quad y^+ = g(x^+)\eta \to 0 \tag{2.43}$$

$$\frac{\partial u^+}{\partial y^+} \leq C \quad \text{for} \quad y^+ = g(x^+)\eta \to 0 \tag{2.44}$$

for an upper bound $C \in \mathbb{R}$. The limit $y^+ \to 0$ implies that $\eta \to 0$ since $y^+ = g(x^+)\eta$ and g satisfies $g(0) = e^1$ and is bounded for fixed $x^+ > 0$. First we consider (2.43) and from equation (2.8) we obtain the relation

$$v^+ = -\underbrace{S'\eta g}_{\to 0} + \underbrace{\frac{1}{\kappa} g'\,(\eta F' - F)}$$

The first term on the right hand side goes to zero as $\eta \to 0$, since g is bounded for every fixed $x^+ > 0$. Regarding the second term, $F'(0)$ is finite and therefore $\eta F' \to 0$ as $\eta \to 0$, and we mention that g' is bounded for every fixed $x^+ > 0$. Therefore Alber [1980] proposes to impose $F_0 = 0$ for $\eta = 0$ in order to ensure that $v^+ \to 0$ as $\eta \to 0$. An additional boundary conditions follows from the condition that $\partial U/\partial y$ remains bounded for $\eta \to 0$, see (2.44). Then from equation (2.7) we infer that F'' needs to be bounded for $\eta \to 0$ and Alber [1980] proposes the condition that $\eta F_0\,''(\eta)$ for $\eta \to 0$. Then the boundary conditions for $\eta \to 0$ are

$$F_0(0) = 0\ , \qquad \lim_{\eta \to 0, \eta > 0} \eta F_0\,''(\eta) = 0 \tag{2.45}$$

The equations (2.41) and (2.42) are second order ordinary differential equations for F_0' and F_1'. Therefore two boundary conditions are needed for F_i'. An additional boundary condition follows from matching the solution to the log-law for large y^+-values (at fixed x^+). Using (2.4), Alber [1980] proposes

$$\lim_{\eta \to \infty} F_0(\eta)' \to \log(\eta) + B\kappa \tag{2.46}$$

For the boundary conditions for F_1, Alber [1980] imposes

$$F_1(0) = 0, \qquad \lim_{\eta \to 0, \eta > 0} \eta F_1\,'(\eta) = 0, \qquad \lim_{\eta \to \infty} F_1\,'(\eta) = 0\ . \tag{2.47}$$

2.7 Solution of similarity equation for $F_0(\eta)$

Then Alber [1980] first solves the problem for F_0, i.e., (2.41). This first order ordinary differential equation (2.41) needs a single boundary condition to specify the solution and Alber [1980] uses the second condition in (2.45). Integration of the linear ordinary differential equation over η with the substitution $\mathcal{G} = \eta F_0\,''$ yields

$$[\eta F_0\,'']' + [\eta F_0\,''] - 1 = 0 \quad \Leftrightarrow \quad \mathcal{G}' = 1 - \mathcal{G}, \quad \text{with} \quad \mathcal{G} = \eta F_0\,'' \tag{2.48}$$

subject to the boundary condition $\mathcal{G}(0) = 0$.

2.7.1 Solution by transformation of variables

We write this as a linear inhomogeneous differential equation

$$\mathcal{G}\,' = f(x)\,\mathcal{G} + g(x), \quad f(x) = -1, \quad g(x) = 1 \tag{2.49}$$

The solution of the corresponding homogeneous problem $\mathcal{G}\,' = f(x)\,\mathcal{G}$ is

$$\mathcal{G}(x) = \lambda\, e^{F(x)} \tag{2.50}$$

with $F(x) = -x$ which satisfies $F\,' = f = -1$. This gives us

$$\mathcal{G}(x) = \lambda\, e^{-x} \tag{2.51}$$

Using the method of variation of constants we obtain the following general form for the solution of the inhomogeneous problem

$$\mathcal{G}(x) = c\, e^{F(x)} + H(x)\, e^{F(x)}\ , \qquad c \in \mathbb{R} \tag{2.52}$$

where $H(x)$ is the integral of $g(x)\, e^{-F(x)}$. Therefore

$$H\,' = g(x)\, e^{-F(x)} = e^{-(-x)} = e^{x} \tag{2.53}$$

and we find that

$$H(x) = e^{-F(x)} = e^{x} \tag{2.54}$$

By substitution into (2.52) we obtain

$$\mathcal{G}(x) = c\, e^{-x} + e^{x}\, e^{-x} = c\, e^{-x} + 1 \tag{2.55}$$

We determine the free constant c by imposing the boundary condition $\mathcal{G}(0) = 0$.

$$\mathcal{G}(0) = c\, e^{-0} + 1 = 0 \quad \Leftrightarrow \quad c = -1 \tag{2.56}$$

We substitute this relation into (2.55) and obtain

$$\mathcal{G}(x) = \left(1 - e^{-x}\right) \tag{2.57}$$

2.7.2 Solution for $F_0\,''$

The solution for $\mathcal{G}(x)$ is then substituted to find $F_0\,''$

$$F_0\,'' = \frac{(1 - e^{-\eta})}{\eta} \tag{2.58}$$

2.7.3 Similarity solution for $F_0(\eta)'$ and matching

To determine $F_0\,'$, (2.58) is integrated again over η

$$F_0\,'(\eta) = F_0\,'(0) + \int_0^{\eta} \left[\frac{1 - e^{-t}}{t}\right] \mathrm{d}t \tag{2.59}$$

Then Alber [1980] rearranges the arising integral as

$$\begin{aligned}\int_0^\eta \left[\frac{1-e^{-t}}{t}\right]\mathrm{d}t &= \int_0^\eta \frac{1}{t}\mathrm{d}t - \int_0^\eta \frac{e^{-t}}{t}\mathrm{d}t \\ &= \log(\eta) - \log(0) - \int_0^\infty \frac{e^{-t}}{t}\mathrm{d}t + \int_\eta^\infty \frac{e^{-t}}{t}\mathrm{d}t \\ &= \log(\eta) - \log(0) + \log(0) + \gamma + \int_\eta^\infty \frac{e^{-t}}{t}\mathrm{d}t \\ &= \log(\eta) + \gamma + \int_\eta^\infty \frac{e^{-t}}{t}\mathrm{d}t\end{aligned}$$

Therein we use the rule of integration by parts within the following side calculation

$$\begin{aligned}\int_0^\infty \underbrace{\frac{1}{t}}_{=f'}\underbrace{e^{-t}}_{=g}\mathrm{d}t &= \left[\log(t)e^{-t}\right]_0^\infty - \underbrace{(-)\int_0^\infty \log(t)e^{-t}\mathrm{d}t}_{=\gamma} \\ &= \underbrace{\lim_{t\to\infty}\log(t)e^{-t}}_{=0} - \log(0)e^{-0} - \gamma = -\log(0) - \gamma \qquad (2.60)\end{aligned}$$

where γ is Euler's constant 0.5772157. i.e.,

$$\gamma = -\int_0^\infty \log(t)e^{-t}\mathrm{d}t \qquad (2.61)$$

By using this relation Alber [1980] writes $F_0{}'$ as

$$F_0{}' = F_0{}'(0) + \gamma + \log(\eta) + E_1(\eta), \qquad \text{with} \qquad E_1(\eta) = \int_\eta^\infty \frac{e^{-t}}{t}\mathrm{d}t \quad (2.62)$$

where the value of the integration constant $F'(0)$ needs to be determined. Following Alber [1980], the value of $F'(0)$ is determined by matching using the asymptotic boundary condition (2.46)

$$\begin{aligned}&\lim_{\eta\to\infty} F_0{}'(\eta) = \log(\eta) + B\kappa \\ &\lim_{\eta\to\infty} F_0{}'(\eta) = F_0{}'(0) + \gamma + \log(\eta) + \underbrace{\lim_{\eta\to\infty} E_1(\eta)}_{=0} = \log(\eta) + B\kappa \\ \Leftrightarrow \qquad &F_0{}'(0) = \gamma + B\kappa\end{aligned}$$

Putting this together yields the following first order approximation $F_0{}'(\eta)$

$$F_0{}'(\eta) = \log(\eta) + E_1(\eta) + B\kappa \qquad (2.63)$$

Alber [1980] points out the finite slope of $F_0{}'$ at $\eta = 0$ and the asymptotic form, i.e., $F_0{}'$ is approaching $B\kappa + \log(\eta)$ as $\eta \to \infty$.

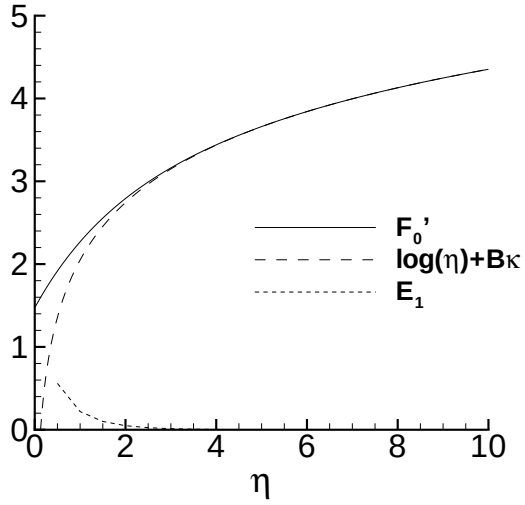

Figure 2.3: Velocity profile function F_0' in similarity scaling.

2.8 Discussion of asymptotic behaviour

Figure 2.3 provides some illustration for the function $F_0{}'$. Moreover it shows its contributions, $\log(\eta)$ and E_1. The asymptotic behaviour $F_0{}'$ and the way it approaches $\log(\eta)$ for $\eta \to \infty$ is shown. Additionally the perturbation E_1 of the log-law is shown. It describes how the inner part of the log-law is eaten up by the wake and which region of the log-law has been eroded.

The function $F_0{}'$ is plotted in similarity scaling versus $\eta = y^+/g$. We observe that $F_0{}'$ follows the log-law for $\eta > 2$. Clearly E_1 becomes negligible for $\eta > 2$. For $1 < \eta < 2$, the contribution of E_1 is small, but not negligible. For $\eta < 1$ the contribution of E_1 is significant and changes the behaviour of $F_0{}'$ qualitatively compared to the log-law behaviour.

2.8.1 Matching arguments

Now we attempt to give some illustration. We consider the example that the turbulent boundary layer is at $\delta_{99}^+ = 10000 = Re_{\tau,\mathrm{T.E.}}$. Then the outer edge of the log-layer is at $y^+ \approx 1500$ near the trailing edge. From figure 2.2 we observe that, at $x^+ = 20000 = 2\delta_{99}^+$, the value of g is $g \approx 500$. For a rough discussion and illustration, we make a simplification. We assume for the moment that the flow is parallel to the x-axis and that the outer edge of the log-law remains at a fixed y^+-position in the wake (which is, of course, not correct). We consider the point at x^+ with a distance y^+ from the centerline. Then the outer edge of the log-law remnant in the wake would still be at $y^+ = 1500$. For $\delta_{99}^+ = 10000$, we then obtain $\eta = y^+/g = 3$ for this distance from the centerline. Therefore an unaltered log-law remnant should be visible in the region $2 < \eta < 3$. This region is therefore sufficiently thick to be visible from experimental data. At $x^+ = 40000 = 4\delta_{99}^+$, the value of g is $g \approx 1000$. Therefore the position $y^+ = 1500$ corresponds now to $\eta = y^+/g = 1.5$. We conclude from figure 2.3 that for

$x^+ = 4\delta_{99}^+$ the perturbation E_1 should be visible and an unaltered log-law can no longer be observed. Of course, this argument is simplified, as the wake is spreading in downstream direction. However, this simple argument can serve for some understanding to assess the qualitative implication of the analytical form of $F_0\,'$.

2.9 The centerline velocity in the near wake

The first order approximation for the wake centerline velocity in region II can be written as

$$u_{\mathrm{CL}}^+(x^+) \equiv u^+(x^+, 0) = S(x^+) + \frac{1}{\kappa} F_0\,'(0) = \frac{1}{\kappa} \log g(x^+) + \frac{\gamma}{\kappa} + B \quad (2.64)$$

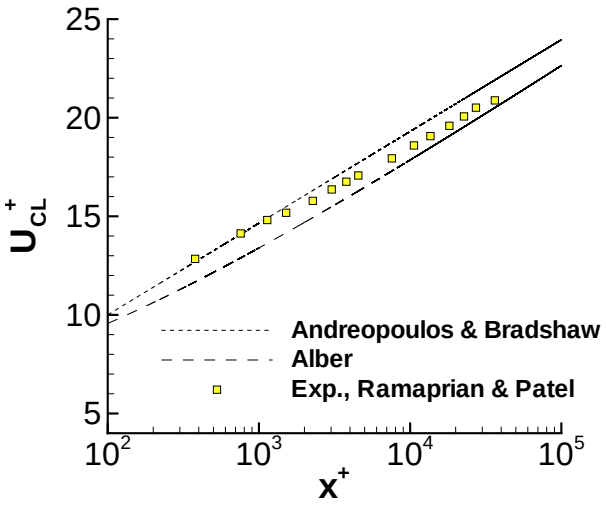

Figure 2.4: Streamwise evolution of centerline velolicity. Comparison of theoretical results and experimental data.

The approximative empirical result by Andreopoulos and Bradshaw [1980] (following Ramaprian et al. [1982]) is

$$u_{\mathrm{CL}}^+(x^+) = 2.02 \log(x^+) + 0.7 \quad (2.65)$$

The observation that $\log(g(x^*)) \approx 0.8(\log(x)+1)$ and using $\kappa = 0.4$ can be used in Bradshaw's relation to obtain

$$u_{\mathrm{CL}}^+(x^+) = 2.02 \log(x^*) + 0.7 \approx 0.8 \frac{1}{\kappa} \log(x^+) + C' \quad (2.66)$$

Therefore the thickness of the inner wake $g(x^+)$ grows like $(x^+)^{4/5}$

$$g(x) \ \sim x^{4/5} \quad (2.67)$$

and it seems interesting that the streamwise growth of the turbulent boundary layer at ZPG can be approximately described as $\sim x^{4/5}$, see Durbin and Reif [2001] p.77.

2.9.1 Solution for $F_0(\eta)$

To determine F_0, we use integration once more with respect to η. The idea is to use the relation

$$F_0(\eta) - \underbrace{F_0(0)}_{=0} = \int_0^\eta 1\, F_0{}'\mathrm{d}\eta$$

which uses the boundary condition $F_0(0) = 0$, and then to use the rule of integration by parts. For this purpose we recall that

$$[fg]_a^b = \int_a^b [fg]'\mathrm{d}x = \int_a^b f'g\mathrm{d}x + \int_a^b fg'\mathrm{d}x \tag{2.68}$$

and we apply this rule as follows

$$\int_a^b \underbrace{f'}_{=1}\underbrace{g}_{=F_0'}\mathrm{d}x = [\underbrace{f}_{=\eta}\underbrace{g}_{=F_0'}]_a^b - \int_a^b \underbrace{f}_{=\eta}\underbrace{g'}_{=F_0''}\mathrm{d}x \tag{2.69}$$

We use that F_0'' is given by (2.58) and the boundary condition $F_0(0) = 0$ and obtain

$$\begin{aligned} F_0(\eta) - \underbrace{F_0(0)}_{=0} &= \int_0^\eta 1\, F_0{}'\mathrm{d}\eta = [\eta F_0{}']_0^\eta - \int_0^\eta \eta\, F_0{}''\mathrm{d}\eta \\ &= \eta F_0{}'(\eta) - \underbrace{0F_0{}'(0)}_{=0} - \int_0^\eta \eta\left[\frac{1}{\eta}\left(1-e^{-\eta}\right)\right]\mathrm{d}\eta \\ &= \eta\left[B\kappa + \log(\eta) + E_1(\eta)\right] - \int_0^\eta \left(1-e^{-\eta}\right)\mathrm{d}\eta \end{aligned}$$

We use the following side calculation for the second integral

$$\begin{aligned} -\int_0^\eta \left(1-e^{-\eta}\right)\mathrm{d}\eta &= -[\eta]_0^\eta + \int_0^\eta e^{-\eta}\mathrm{d}\eta = -\eta + \left[-e^{-\eta}\right]_0^\eta \\ &= -\eta + \left[-e^{-\eta} - (-1)\right] = 1 - \eta - e^{-\eta} \end{aligned}$$

Putting these calculations together, we obtain the result for F_0 that (see eq. (55) of Alber [1980])

$$F_0(\eta) = \eta\left[\log(\eta) + E_1(\eta) + B\kappa - 1\right] + \left[1 - e^{-\eta}\right] \tag{2.70}$$

2.9.2 Integration of the similarity equation for $F_1(\eta)$

The similarity equation (2.42) for F_1 reads

$$\left[\eta F_1{}''\right]' + \left[\eta F_1{}''\right] = \left[F_0{}' - \eta F_0{}'' - F_0 F_0{}''\right] \tag{2.71}$$

We substitute the solution for F_0, F_0', and F_0'' and obtain

$$\begin{aligned}
&[\eta F_1\,'']' + [\eta F_1\,''] \\
&= [F_0\,' - \eta F_0\,'' - F_0 F_0\,''] \\
&= [B\kappa + \log(\eta) + E_1(\eta)] - \left[\eta \frac{1-e^{-\eta}}{\eta}\right] \\
&\quad - \left[\eta\,(\log(\eta) + E_1(\eta) + B\kappa - 1) + \left(1-e^{-\eta}\right)\right]\left[\frac{1-e^{-\eta}}{\eta}\right] \\
&= [B\kappa + \log(\eta) + E_1(\eta)] - \left(1-e^{-\eta}\right) \\
&\quad - [\log(\eta) + E_1(\eta) + B\kappa - 1]\left(1-e^{-\eta}\right) - \left(1-e^{-\eta}\right)\left[\frac{1-e^{-\eta}}{\eta}\right] \\
&= [B\kappa + \log(\eta) + E_1(\eta)] - \left(1-e^{-\eta}\right) \\
&\quad - [\log(\eta) + E_1(\eta) + B\kappa - 1]\left(1-e^{-\eta}\right) - \frac{\left(1-e^{-\eta}\right)^2}{\eta} \\
&= [B\kappa + \log(\eta) + E_1(\eta)] - \left(1-e^{-\eta}\right) - [\log(\eta) + E_1(\eta) + B\kappa - 1] \\
&\quad + [\log(\eta) + E_1(\eta) + B\kappa - 1]\,e^{-\eta} - \frac{\left(1-e^{-\eta}\right)^2}{\eta} \\
&= + [\log(\eta) + E_1(\eta) + B\kappa - 1]\,e^{-\eta} - \frac{\left(1-e^{-\eta}\right)^2}{\eta} + e^{-\eta} \\
&= + [\log(\eta) + E_1(\eta) + B\kappa]\,e^{-\eta} - \frac{\left(1-e^{-\eta}\right)^2}{\eta}
\end{aligned}$$

This gives the following equation for F_1''

$$[\eta F_1\,'']' + [\eta F_1\,''] = [\log(\eta) + E_1(\eta) + B\kappa]\,e^{-\eta} - \frac{\left(1-e^{-\eta}\right)^2}{\eta} \tag{2.72}$$

Alber [1980] gives the solution for F_1'' as

$$F_1'' = F_0(\eta)\frac{e^{-\eta}}{\eta} + [E_1(\eta) - E_i(\eta) + 2(\log(\eta) + \gamma)]\frac{e^{-\eta}}{\eta} \tag{2.73}$$

where E_i denote the following version of the exponential integral

$$E_i(\eta) = -\int_{-\eta}^{\infty} \frac{e^{-t}}{t}\mathrm{d}t \tag{2.74}$$

According to Alber [1980], the dominant term in (2.73) contains $E_i(\eta)$. He states that

$$\lim_{\eta\to\infty} E_i(\eta) \sim \frac{e^{\eta}}{\eta} \tag{2.75}$$

Therefore

$$F_1'' \sim E_i(\eta)\frac{e^{-\eta}}{\eta} \sim \frac{e^{\eta}}{\eta}\frac{e^{-\eta}}{\eta} = \frac{1}{\eta^2} \quad \Leftrightarrow \quad F_1' \sim \frac{1}{\eta} \tag{2.76}$$

and by integration $F_1 \sim \log(\eta) + C$.

Chapter 3

Comparison with experimental data by Ramaprian & Patel

3.1 Description of the experiment

This chapter is dedicated to a comparison of the predictions by Alber and the experimental results for the symmetric wake of a flat plate and its turbulent boundary layer by Ramaprian et al. [1982]. They performed experiments using a 1.829 m long flat plate in a wind tunnel of cross-section 1.6 × 1.6 m. The measurements were at a nominal wind-speed of $U_\infty = 22\,\mathrm{m/s}$. The paper by Ramaprian et al. [1982] specifies for the flow conditions that at a station 76.2 mm upstream of the trailing edge of the flat plate, the boundary data were $\delta_{99} = 34\,\mathrm{mm}$, $Re_{\delta^*} = U_\infty \delta^*/\nu = 6790$, $Re_\theta = U_\infty \theta/\nu = 5220$, shape factor $H = 1.29$, and $c_f = 0.0029$. From c_f and U_∞, we infer $u_\tau = 0.838\,\mathrm{m/s}$ and $\delta_{99}^+ = \delta_{99} u_\tau/\nu = 1887$.

3.2 Results

We show the predicted mean velocity profile for F_0 and for $F_0 + \log(g)^{-1} F_1$ in figures 3.1-3.3. At $x = 6.35\,\mathrm{mm}$, corresponding to $x/\delta_{99} = 0.19$, the log-law is still alive almost unaltered in the inner part of the wake near the wake centerline. For $x = 38.1\,\mathrm{mm}$, corresponding $x/\delta_{99} = 1.1$, the inner part of the log-law is already eroded, but the log-law remains unaltered in the outer part of the inner wake. We also include the velocity profile at $x = 6.35\,\mathrm{mm}$ to illustrate how the inner part of the log-law is altered. We see that the theoretical profiles by Alber for F_0 and for $F_0 + \log(g)^{-1} F_1$ can described the experimental data really good. Note that u^* used for +-units denotes the friction velocity at the trailing edge.

At $x = 76.2\,\mathrm{mm}$, corresponding to $x/\delta_{99} = 2.2$ (see figure 3.2 (left)) and at $x = 177.8\,\mathrm{mm}$ (see figure 3.2 (right)), corresponding to $x/\delta_{99} = 5.2$ the log-law has been altered completely, except near the outer edge of the log-law region.

At $x = 609.6\,\mathrm{mm}$, or $x/\delta_{99} = 17$, the log-law can no longer be observed.

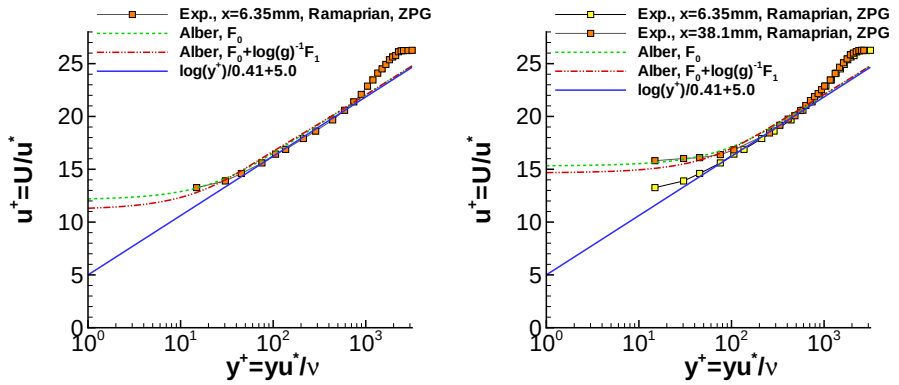

Figure 3.1: Behaviour of mean velocity profiles in the wake at $x = 6.35\,\mathrm{mm}$ (left) and at $x = 38.1\,\mathrm{mm}$ (right).

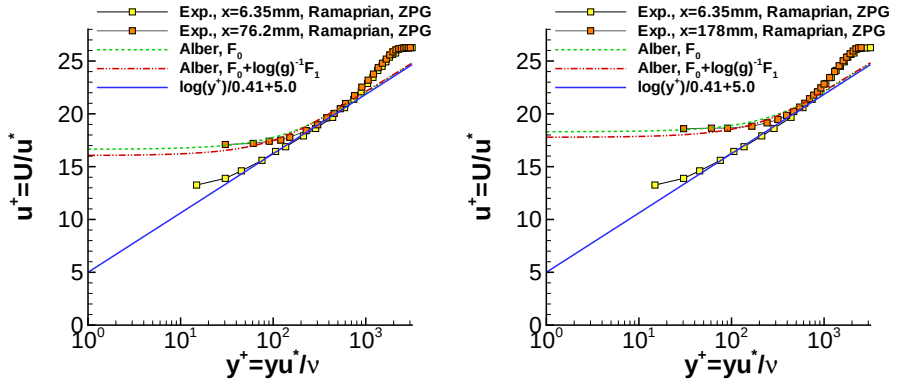

Figure 3.2: Behaviour of mean velocity profiles in the wake at $x = 76.2\,\mathrm{mm}$ (left) and at $x = 177.8\,\mathrm{mm}$ (right).

We are no longer in the near wake described by the theory by Alber. However we find the the perturbed solutions $F' = F_0{}'$ and $F' = F_0 + \log(g)^{-1}F_1$ can describe the mean velocity profile surprisingly well.

To summarize, we find that the approximation $F' = F_0{}'$ already gives a good approximation of the experimental data. The change of the mean-velocity profile in the inner 15% of the wake can be described both qualitatively and quantitatively really good. The importance of the correction by taking into account $F_1{}'$ is not easily assessed.

The sources of uncertainties stem from the uncertainties associated with the wind-tunnel experiment. One aspect are the uncertainties in the experimental data, e.g., in the accuracy of u_τ, as u_τ is appearing due to the scaling of the mean velocity profiles. Other aspects are the flow conditions. Whereas in a numerical experiment, a two-dimensional flow can be realized, in the wind tunnel the effects of the side walls of the wind tunnel arise. Moreover, it is a challence to ensure perfectly symmetric onflow conditions at incidence angle $\alpha = 0°$ for the splitter plate.

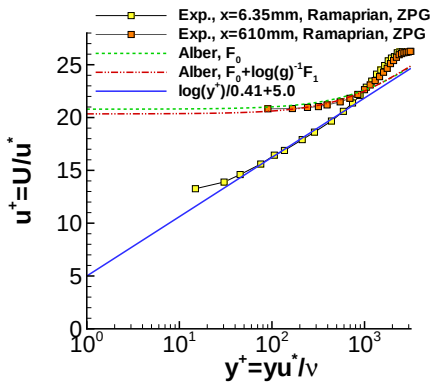

Figure 3.3: Behaviour of mean velocity profiles in the wake at $x = 609.6\,\mathrm{mm}$.

Chapter 4

Conclusion and outlook

The present work re-visited the analytical work by Alber [1980] for the near wake region of the wake of a long flat plate and its turbulent boundary layer. The ultimate goal is to extend this work for adverse pressure gradients. Due to the large number of mathematical details, the first step was to review the work by Alber [1980] carefully.

At a first attempt, it was seen that the extension for adverse pressure gradients of the work by Alber [1980] is by far not straight forward. For strong adverse pressure gradients, the similarity ansatz by Alber [1980] might need modification. On the one hand, the centerline velocity can be expected to depend on the pressure gradients. On the other hand, the velocity at the outer edge of the wake, where the flow approaches inviscid irrotational flow, is decreasing as the flow experiences an adverse pressure gradient.

Acknowledgement

This project of the author together with Prof. R. Radespiel and Dr. P. Scholz from ISM and with Prof. M. Strelets from SPbPTU is funded by DFG and the Russian Foundation for Basic Research (RFBR) under Grant No. RA 595/26-1, KN 888/3-1 and No. 17-58-12002, which is gratefully acknowledged. The contribution of the second author Christopher Scholl from Georg-August Universität Göttingen was during his internship in August and September 2018. The authors are grateful to Dr. Fritz Kießling for his valuable assistance for this work. Thanks are also to Paul Korsmeier for proof reading parts of this report.

Appendix A

Appendix

A.1 Ordinary differential equations

First we consider the differential equation which is linear in y and homogeneous

$$y' = f(x)y \tag{A.1}$$

The solution is found as follows

$$\begin{aligned}
& y' &=& f(x)y \\
\Leftrightarrow \quad & \frac{y'}{y} &=& f(x) \\
\Leftrightarrow \quad & [\log(y)]' &=& f(x) \\
\Leftrightarrow \quad & \log(y) &=& \int_0^x f(x)\mathrm{d}x + c \\
\Leftrightarrow \quad & y = e^{\log(y)} &=& e^c e^{\int_0^x f(x)\mathrm{d}x} \\
\Leftrightarrow \quad & y &=& \lambda e^{\int_0^x f(x)\mathrm{d}x} \\
\Leftrightarrow \quad & y &=& \lambda\, e^{F(x)}\,, \qquad F(x) = \int_0^x f(x)\mathrm{d}x
\end{aligned}$$

Then we consider the differential equation which is linear in y and inhomogeneous

$$y' = f(x)y + g(x) \tag{A.2}$$

For the solution, the first step is to start with the soltion of the corresponding homogeneous equation $y' = f(x)y$ with the solution $y = \lambda e^{F(x)}$ with $\lambda \in \mathbb{R}$ and $F' = f$. Then for the solution of the inhomogenous problem we make the ansatz

$$y(x) = \lambda(x) e^{F(x)} \tag{A.3}$$

with an unknown function $\lambda(x)$ which has to be determined. (For this reason the method is called "variaton of constant"). Then the substitution of the ansatz

into the differential equation gives

$$\begin{aligned} y' &= f(x)y + g(x) \\ \left[\lambda(x)e^{F(x)}\right]' &= f(x)\left[\lambda(x)e^{F(x)}\right] + g(x) \\ \Leftrightarrow \quad \lambda'(x)e^{F(x)} + \lambda(x)e^{F(x)}f(x) &= f(x)\lambda(x)e^{F(x)} + g(x) \\ \Leftrightarrow \quad \lambda'(x)e^{F(x)} &= g(x) \\ \Leftrightarrow \quad \lambda'(x) &= e^{-F(x)}g(x) \\ \Leftrightarrow \quad \lambda(x) &= H(x) + c, \quad H' = g(x)e^{-F(x)} \end{aligned}$$

where $c \in \mathbb{R}$. Then the general solution is given by

$$y(x) = c\, e^{F(x)} + H(x)\, e^{F(x)}, \qquad c \in \mathbb{R} \tag{A.4}$$

A.2 Transformation rule for integration

Substitution rule for integration

$$\int_a^b f(\phi(t))\phi'(t)\mathrm{d}t = \int_{\phi(a)}^{\phi(b)} f(x)\mathrm{d}x \tag{A.5}$$

which follows immediately from

$$\begin{aligned} \int_a^b f(\phi(t))\phi'(t)\mathrm{d}t &= \int_a^b F'(\phi(t))\phi'(t)\mathrm{d}t = [F \circ \phi]_a^b \\ &= F(\phi(b)) - F(\phi(a)) = \int_{\phi(a)}^{\phi(b)} f(x)\mathrm{d}x \int_{\phi(a)}^{\phi(b)} f(x)\mathrm{d}x \end{aligned}$$

where we used F with $F' = f$. As an example, the goal is to integrate

$$\int_0^a \sin(\underbrace{2x}_{=t})\mathrm{d}x \tag{A.6}$$

Then define the transformation

$$t(x) = 2x, \qquad x = \frac{1}{2}t, \qquad \mathrm{d}x = \frac{1}{2}\mathrm{t} \tag{A.7}$$

The bounds for integration transform

$$x_1 = 0 \to t_1(x_1) = 2x_1 = 0, \qquad x_2 = 0 \to t_2 = 2x_2 = 0 \tag{A.8}$$

$$\begin{aligned} \int_0^a \sin(\underbrace{2x}_{=t})\mathrm{d}x &= \int_{\phi(0)}^{\phi(a)} \sin(t)\frac{1}{2}\mathrm{d}t = \int_0^{2a} \sin(t)\frac{1}{2}\mathrm{d}t \\ &= \frac{1}{2}\left[-\cos(t)\right]_0^{2a} = \frac{1}{2}\left[-\cos(2a) + 1\right] \end{aligned} \tag{A.9}$$

A.3 Integration by parts

$$[fg]_a^b = \int_a^b [fg]'\mathrm{d}x = \int_a^b f'g\mathrm{d}x + \int_a^b fg'\mathrm{d}x \tag{A.10}$$

Bibliography

I. E. Alber. Turbulent wake of a thin, flat plate. *AAIA J.*, 18:1044–1051, 1980.

J. Andreopoulos and P. Bradshaw. Measurement of Interacting Turbulent Shear Layers in the Near Wake of a Flat Plate. *J. Fluid Mech.*, 100:639–668, 1980.

E. A. Bogucz and J. D. A. Walker. The turbulent near wake at a sharp trailing edge. *J. Fluid Mech.*, 196:555–584, 1988.

W. Breitenstein, P. Scholz, R. Radespiel, M. Burnazzi, T. Knopp, E. Guseva, M. Shur, and M. Strelets. A wind tunnel experiment for symmetric wakes in adverse pressure gradients. *AIAA Paper 2019-1875*, 2019.

M. Burnazzi, T. Knopp, M. Strelets, M. Shur, A. Travin, W. Breitenstein, P. Scholz, and R. Radespiel. Characterization of off-surface separation caused by adverse pressure gradient in a turbulent wake. In *21th STAB/DGLR Symposium on New Results in Numerical and Experimental Fluid Mechanics. 21. STAB/DGLR Symposium 2018, 6.-8. Nov. 2018, Darmstadt, Deutschland*, 2018.

S. X. Ying C. L. Rumsey. Prediction of high lift: review of present CFD capability. *Prog. Aerosp. Sci.*, 38:145–180, 2002.

R. Chevray and L. S. G. N. Kovasznay. Turbulence measurements in the wake of a thin flat plate. *AAIA J.*, 7:1641–1643, 1969.

D. M. Driver and G. G. Mateer. Wake flow in adverse pressure gradient. *Int. J. Heat Fluid Flow*, 23:564–571, 2002.

P. A. Durbin and B. A. Petterson Reif. *Statistical theory and modelling for turbulent flows*. John Wiley & Sons, Chichester, 2001.

E. Guseva, M. Strelets, A. Travin, M. Burnazzi, and T. Knopp. Zonal rans-iddes and rans computations of turbulent wake exposed to adverse pressure gradient. *Journal of Physics: Conference Series*, 1135:012092, 2018.

E. Guseva, M. Shur, M. Strelets, A. Travin, W. Breitenstein, R. Radespiel, P. Scholz, M. Burnazzi, and T. Knopp. Experimental/numerical study of turbulent wake in adverse pressure gradient. In Yannick Hoarau, Shia-Hui Peng, Dieter Schwamborn, Alistair J. Revell, and Charles Mockett, editors, *7th Symposium on Hybrid RANS-LES Methods*, volume 143 of *Notes on Numerical Fluid Mechanics and Multidisciplinary Design*, pages 401–412. Springer International Publishing, 2019. Print ISBN 978-3-030-27606-5 Online ISBN 978-3-030-27607-2.

T. Knopp. A new wall-law for adverse pressure gradient flows and modification of k-ω type RANS turbulence models. *AIAA Paper 2016-0588*, 2016.

T. Knopp, N. Reuther, M. Novara, E. Schülein, D. Schanz, A. Schröder, and C. J. Kähler. Investigation of a turbulent boundary layer flow at high Reynolds number using particle-imaging and implications for RANS modeling. In *Tenth International Symposium on Turbulence and Shear Flow Phenomena (TSFP10) July 6-9, 2017, Swissotel, Chicago-IL, USA*, 2017.

T. Knopp, M. Novara, D. Schanz, R. Geisler, F. Philipp, A. Schröder, C. Willert, and A. Krumbein. Modification of the ssg/lrr-omega rsm for turbulent boundary layers at adverse pressure gradient with separation using the new dlr victoria experiment. In *New Results in Numerical and Experimental Fluid Mechanics. Contributions to the 21th STAB/DGLR Symposium Darmstadt, Germany 2018*, 2018.

B. R. Ramaprian, V. C. Patel, and M. S. Sastry. The Symmetric Turbulent Wake of a Flat Plate. *AAIA J.*, 20:1228–1235, 1982.

J. L. Robinson. Similarity solutions in several turbulent shear flows. Technical Report NPL AERO REPORT 1242 A.R.C. 29 330, F.M. 3874., Aeronautical Research Council, 1967.

C. L. Rumsey and T. B. Gatski. Recent Turbulence Model Advances Applied to Multielement Airfoil Computations. *J. Aircraft*, 38(5):904–910, 1999.

S. X. Ying, F. W. Spaid, C. B. McGinley, and C. L. Rumsey. Investigation of Confluent Boundary Layers in High-Lift Flows. *J. Aircraft*, 36(3):550–562, 1996.